LES tutorial for Ocean 3D+1 MURI

Tamay Özgökmen, University of Miami

Contents

1 A Discussion of Ocean Modeling Approaches **2**

2 Large Eddy Simulation **4**

2.1 The Concept of Spatial filtering 6

2.2 Eddy Viscosity SGS models 8

2.2.1 Smagorinsky SGS model: 8

2.3 Approximate deconvolution SGS models 13

2.3.1 Repeated filtering AD model: 13

2.3.2 Rational AD model: 14

2.4 Examples of LES 15

2.4.1 What constitutes a good test problem? 15

2.4.2 Quantification of mixing: 16

2.4.3 What resolution constitutes an LES? 16

3 FTLEs from LES **21**

3.1 Application to Lock Exchange Problem 21

3.2 Application to Mixed Layer Instability 22

1 A Discussion of Ocean Modeling Approaches

Traditional ocean general circulation models (OGCMs) have the advantage that they are already configured at the global scale, as well as for specific ocean basins by national operational centers, such as Naval Research Laboratory (NRL) and National Center for Environmental Prediction (NCEP)[1]), with mesh spacings going down to about 5 km. OGCMs can also be set up for regional simulations at finer resolutions (Capet et al., 2008). The primary advantage of these approaches is that the dynamics of the general circulation and mesoscale features such as jets and eddies are well captured. These OGCMs contain realistic forcing, domain geometry, and assimilate ocean data.

There are however several disadvantages of OGCMs for simulating submesoscale flows:

- First, the equation set (so-called primitive equations, PE) contains the hydrostatic approximation, which is justified by the high aspect ratio between horizontal and vertical domain dimensions. The hydrostatic approximation becomes invalid for scales below approximately 1 km (Kantha and Clayson, 2000), or within the submesoscale range. The breakdown of the hydrostatic approximation creates two types of errors in OGCMs. Internal waves are prominent features in the ocean with well-known dispersion relations and characteristics (Garrett and Munk, 1972). It is known that hydrostatic models cannot produce the correct dispersion for non-linear internal waves, leading to unrealistically fast propagating waves (Scotti and Mitran, 2008). Also, the overturning of density surfaces by Kelvin-Helmholtz instabilities, which are one of the primary mechanisms responsible for mixing in the ocean, cannot be explicitly captured with hydrostatic models. In fact, the accuracy of hydrostatic models can substantially degrade with finer resolution at such scales (Chang et al., 2005). Inclusion of a non-hydrostatic pressure solver in hydrostatic OGCMs requires a substantial change in these codes (Scotti and Mitran, 2008).

- Second, for the reasons described above, OGCMs contain parameterizations for mixing and dissipation (but not for dispersion, to the knowledge of the authors). These parameterizations may range from algebraic models to second-order turbulence closures

[1] http://www.hycom.org/ocean-prediction

(Large, 1998). One challenge with algebraic closures is that they can contain dimensional parameters that need to be tuned for different flow problems (Chang et al., 2005). The turbulence closures have been imported from the engineering community and further developed for stratified oceanic flows (Mellor and Yamada, 1982; Kantha and Clayson, 1994; Burchard and Baumert, 1995; Burchard and Bolding, 2001; Canuto et al., 2001; Baumert and Peters, 2004; Baumert et al., 2005; Warner et al., 2005; Umlauf and Burchard, 2005; Canuto et al., 2007). They have been shown to work well in challenging ocean mixing problems (e.g., Ilıcak et al. (2008)). But perhaps they require more extensive evaluation as more comprenhesive ocean data become available.

- Also, given that the hydrostatic approximation changes the vertical momentum balance, turbulence closures are applied only in the vertical direction. This has created a disconnect between horizontal and vertical closure schemes.

- Third, there are challenges with data assimilation. Assimilation can influence conservation laws. In addition, it is not clear that assimilating data that contain much higher spatial resolution than the OGCMs, or simply point measurements on 5 to 10 km grids would enhance the realism of the model for submesoscale processes.

- Finally, the prevailing OGCMs are based on second order numerics, thereby requiring more mesh points for convergence than higher order methods (Deville et al., 2002). Given that submesoscale processes are expected to be captured near the highest resolved wave number range in OGCMs, it becomes likely that numerical dissipation and dispersion errors could influence submesoscale flow behavior.

As such, it is beneficial to consider methods developed in the computational fluid dynamics (CFD) community for simulating submesoscale flows. While these models are typically not configured to incorporate the large-scale realism of OGCMs, they offer high numerical accuracy, scalability, adaptive and/or unstructured meshes, and integrate the well-established Navier-Stokes or Boussinesq equations (BE) of motion. In that sense, they address many of the issues that create challenges for OGCMs outlined above. Nevertheless, not all CFD methods are appropriate for oceanic problems. The large Reynolds numbers in ocean flows

prohibit the direct numerical simulation (DNS), in which all degrees of freedom are computed. Reynolds averaged Navier Stokes (RANS, Wilcox (1998)) codes are computationally efficient, but raise several questions. First, the decomposition of the flow field into a mean and fluctuating component creates some ambiguity for transient flows, as in the case of mixed layer instability. Second, many RANS closures rely on the eddy viscosity paradigm, or forward cascade of energy, which is not always valid in the presence of stratification, and, in particular, rotation (Vallis, 2006). An alternate approach is the large eddy simulation (LES, Ferziger (2005)), which lies in between the extremes of DNS, in which all turbulence is resolved, and RANS, in which all turbulence is modeled. In regards to the numerical method, the spectral element method (SEM), which combines the geometrical flexibility of finite element method (FEM) with the numerical accuracy of spectral models (Patera, 1984; Maday and Patera, 1989), seems to be ideally suited for submesoscale oceanic flows.

2 Large Eddy Simulation

The fundamental concept behind LES is summarized on page in Fig. 1. LES problem consists of finding the best approximation of u on the computational grid by solving the discrete version of the Navier-Stokes equations. The discrete approach introduces two types of errors:

- *Discretization error* is due to dispersion and dissipation errors introduced by the numerical scheme (finite difference, finite volume, finite element, spectral and spectral element methods).

- *Resolution error* is due to the fact that only a limited number of degrees of freedom can be captured and some scales of the exact solution are missing.

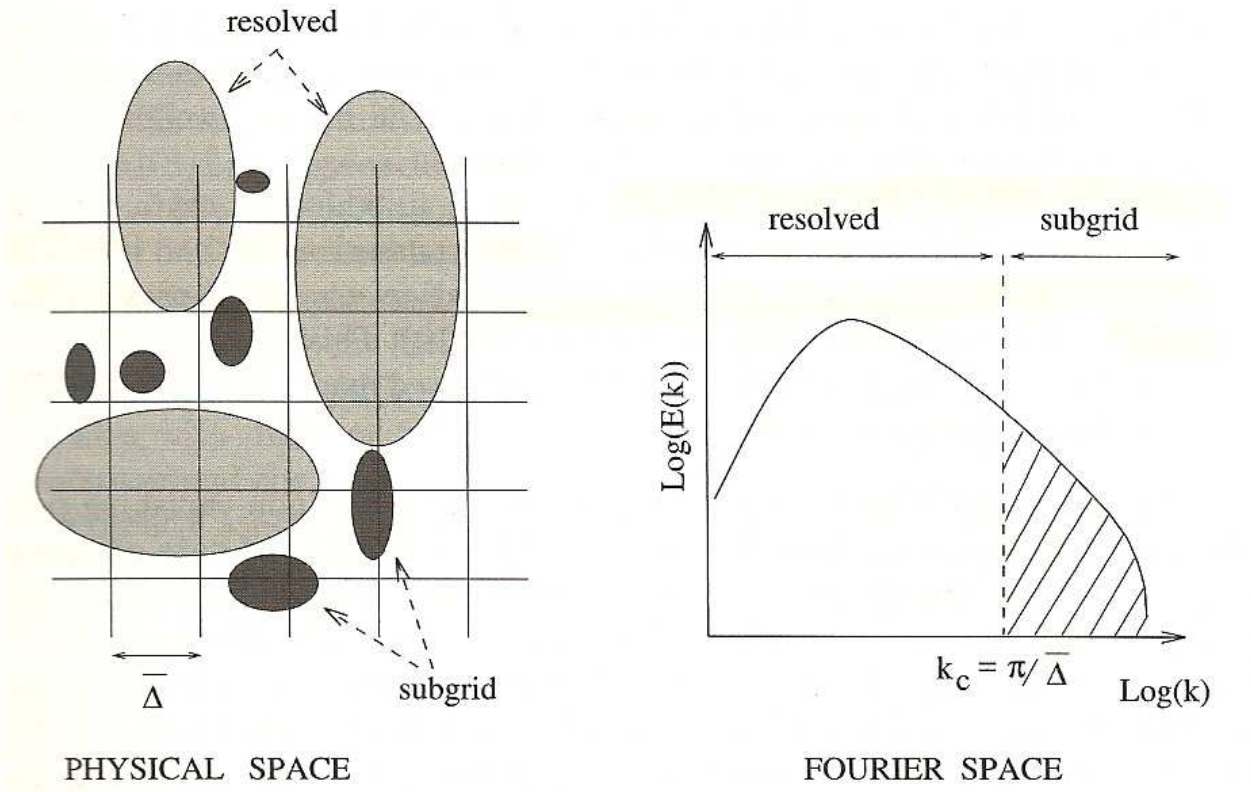

Fig. 1: Schematic view of a simple scale separation operator. From p. 11 of Sagaut (2006).

In LES, we seek the *best* solution by two basic ways:

- *Implicit LES approach* in which the numerical method is such that discretization error and resolution error will cancel one another. There are strong defenders of this approach for control volume based numerical models, such as finite volume and finite elements (Margolin and Rider, 2002), whereas point-wise techniques such as finite differences do not fall into this category.

- *Explicit LES approach* in which extra terms are added to the equations of motion that aim to cancel the resolution error. It is imperative that discretization error must be driven to zero for this approach to work.

In the following, we will focus on the explicit LES approach, under the assumption that high-order models are used to implement LES.

2.1 The Concept of Spatial filtering

The main mathematical idea behind LES is the concept of *spatial filtering*. Consider a generalized filter as a convolution integral, viz.,

$$\begin{aligned} \overline{u}_i(\mathbf{x},t) &= g_\delta \star u_i = \int\int\int g_\delta\,(\mathbf{x}-\xi)u_i(\xi,t)d^3\xi \qquad (1) \\ \overline{u}_i &= u - u_i' \end{aligned}$$

where u_i denotes the full velocity, $\overline{u}$ denotes the resolvable-scale filtered velocity, $u_i' = u_i - \overline{u}_i$ is the subgrid-scale (SGS) velocity, $\delta = (\Delta x \Delta y \Delta z)^{1/3}$ is the filter width as a function of model spatial resolution.

The filter function g_δ is typically of the form top-hat, Gaussian, sharp cut off filters. We will not go into details of such filters, because for most purposes related to actual computations, constraining of the solution on the numerical mesh is assumed to constitute the filtering procedure. Filters are important in situation where the LES solution should be compared to *filtered* DNS solution. It is important to know that unlike Reynolds temporal averaging, the spatial filtering does not commute, leading to:

$$\overline{\overline{u}} = g \star g \star u \neq \overline{u} = g \star u\,, \qquad (2)$$

$$\overline{u'} \neq 0\,, \qquad (3)$$

and therefore, there will be differences regarding the turbulence terms arising from RANS vs LES.

As before, we write the NSE:

$$\frac{\partial u_i}{\partial t} + \frac{\partial}{\partial x_j}(u_i u_j) = -\frac{1}{\rho}\frac{\partial p}{\partial x_i} + \frac{\partial}{\partial x_j}(2\nu S_{ij})\,, \qquad (4)$$

$$\frac{\partial u_i}{\partial x_i} = 0\,, \qquad (5)$$

which, after filtering become

$$\frac{\partial \overline{u}_i}{\partial t} + \frac{\partial}{\partial x_j}(\overline{u_i u_j}) = -\frac{1}{\rho}\frac{\partial \overline{p}}{\partial x_i} + \frac{\partial}{\partial x_j}(2\nu \overline{S}_{ij})\,, \qquad (6)$$

$$\frac{\partial \overline{u}_i}{\partial x_i} = 0\,. \qquad (7)$$

As in the case of RANS, the main issue is the decomposition of the nonlinear term in the momentum equations:

$$\overline{u_i u_j} = \overline{(\overline{u}_i + u'_i)(\overline{u}_j + u'_j)} = \overline{\overline{u}_i \overline{u}_j} + \overline{\overline{u}_i u'_j} + \overline{\overline{u}_j u'_i} + \overline{u'_i u'_j} \,. \tag{8}$$

One approach is to express filtered momentum equation as:

$$\frac{\partial \overline{u}_i}{\partial t} + \frac{\partial}{\partial x_j}(\overline{\overline{u}_i \overline{u}_j}) \;=\; -\frac{1}{\rho}\frac{\partial \overline{p}}{\partial x_i} + \frac{\partial}{\partial x_j}(2\nu \overline{S}_{ij}) - \frac{\partial \tau^*_{ij}}{\partial x_j} \,, \tag{9}$$

where τ^* is so-called *double-decomposition* SGS stress tensor

$$\tau^*_{ij} \;=\; C_{ij} + R_{ij} \,, \tag{10}$$

$$C_{ij} \;=\; \overline{\overline{u}_i u'_j} + \overline{\overline{u}_j u'_i} \,, \tag{11}$$

$$R_{ij} \;=\; \overline{u'_i u'_j} \,, \tag{12}$$

where *cross-stress tensor* C represents the interactions between large and small scales, and the *Reynolds SGS tensor* R reflects the interactions between the sub-grid scales. One problematic issue is that $\overline{\overline{u}_i \overline{u}_j}$ requires (secondary) application of the spatial filter. This issue is remedied by Leonard (1974) who proposed a further decomposition

$$\overline{\overline{u}_i \overline{u}_j} \;=\; (\overline{\overline{u}_i \overline{u}_j} - \overline{u}_i \overline{u}_j) + \overline{u}_i \overline{u}_j \,, \tag{13}$$

$$\;=\; L_{ij} + \overline{u}_i \overline{u}_j \,, \tag{14}$$

where the new L term, called Leonard tensor, represents interactions among the large scales. Using this new decomposition, the filtered momentum equations become

$$\frac{\partial \overline{u}_i}{\partial t} + \frac{\partial}{\partial x_j}(\overline{u}_i \overline{u}_j) \;=\; -\frac{1}{\rho}\frac{\partial \overline{p}}{\partial x_i} + \frac{\partial}{\partial x_j}(2\nu \overline{S}_{ij}) - \frac{\partial \tau_{ij}}{\partial x_j} \,, \tag{15}$$

where τ is so-called *triple-decomposition* SGS stress tensor

$$\tau_{ij} = L_{ij} + C_{ij} + R_{ij} = \overline{u_i u_j} - \overline{u}_i \overline{u}_j \,. \tag{16}$$

We should point out that in the case of a Reynolds operator, $C_{ij} = 0$ and $L_{ij} = 0$ and $\tau_{ij} = R_{ij}$. Therefore, the presence of C_{ij} and L_{ij} constitutes one of the mathematical

differences between RANS and LES. The objective in LES, as in turbulence closure models, is then to come up with SGS models for τ. Note that we have neglected a discussion of SGS models for density perturbation, which appear as

$$\frac{\partial \overline{\rho'}}{\partial t} + \frac{\partial}{\partial x_i}(\overline{u}_i \overline{\rho'}) = +\frac{\partial}{\partial x_i}(K \frac{\partial \overline{\rho'}}{\partial x_i}) - \frac{\partial \sigma}{\partial x_i}\,, \tag{17}$$

$$\sigma = \overline{u\rho'} - \overline{u}\,\overline{\rho'}\,. \tag{18}$$

It is my personal experience (Özgökmen et al., 2007, 2009a, 2009b) that the SGS model for momentum has a much larger influence on the simulation than SGS models for density perturbations, so we will focus only on τ in the following.

Some commonly used models are introduced next. The list is by no means exhaustive. In fact, we will focus only on three SGS models.

2.2 Eddy Viscosity SGS models

2.2.1 Smagorinsky SGS model:

In this model, first the eddy viscosity assumption is made

$$\tau_{ij} = -\nu_{sgs} 2\overline{S}_{ij} = -\nu_{sgs}\left(\frac{\partial \overline{u}_i}{\partial x_j} + \frac{\partial \overline{u}_j}{\partial x_i}\right)\,, \tag{19}$$

where the eddy viscosity coefficient needs to be determined, which is the main contribution of Smagorinsky (1963). We assume high Re homogeneous turbulence with a wide inertial range where the rate of dissipation can be estimated from Taylor's (1935) scaling

$$\varepsilon \sim \frac{Q^3}{L} \sim \frac{q^3}{\delta}\,, \tag{20}$$

where Q is a velocity scale for energetic eddies, L is the integral scale of the turbulence, and q is a typical velocity of the SGS field. We assume that SGS field lives by the energy loss of the large scales and serves to dissipate this energy. The dissipation rate can be using the scaling of its definition

$$\varepsilon \sim \nu_{sgs}\frac{q^2}{\delta^2}\,. \tag{21}$$

From (20) and (21), it follows that

$$\nu_{sgs} \sim q\delta\,, \tag{22}$$

as in the mixing length theory. From (20), (21) and (22), we get

$$\nu_{sgs} \sim Q\delta^{4/3}L^{-1/3}\,. \tag{23}$$

Estimating Q from

$$Q \sim L(\overline{S}_{ij}\overline{S}_{ij})^{1/2} = L|\overline{S}|\,, \tag{24}$$

and inserting a model parameter to produce equality, we have

$$\nu_{sgs} = c_s^2\delta^{4/3}L^{2/3}|\overline{S}|\,, \tag{25}$$

where c_s is so-called Smagorinsky constant. The integral length scale L is not easy estimate, and requires much more complex closures than the one above, as we have seen in sections 4.6 and 4.7. For this reason, the following substitution is used

$$\delta^{4/3}L^{2/3} = \delta^2\,, \tag{26}$$

leading to the Smagorinsky (1963) closure for ν_{sgs}

$$\nu_{sgs} = (c_s\,\delta)^2|\overline{S}|\,, \tag{27}$$

thus

$$\tau_{ij} = -2(c_s\,\delta)^2|\overline{S}|\overline{S}_{ij}\,. \tag{28}$$

The approximation (26) introduces errors into this model and one should not be surprized if the model coefficient is not constant.

Note that unlike RANS turbulence closures, (28) is a function of δ, in a way that

$$\tau_{ij} \to 0 \quad \text{as} \quad \delta \to 0\,, \tag{29}$$

namely LES solution natually becomes DNS in the limit of adequate resolution.

Theoretical estimation of the Smagorinsky constant: The resolved dissipation rate can be estimated from

$$\varepsilon = \nu_{sgs}|\overline{S}|^2 = (c_s\,\delta)^2|\overline{S}|^3\,. \tag{30}$$

Next, we assume that $|\overline{S}|$ can be estimated from the energy spectrum, for which (**??**) applies:

$$\begin{aligned} |\overline{S}|^2 &= 2\int_0^{k_c} k^2 \mathbb{E}(k) dk \approx 2\int k^2 \mathcal{K}\, \varepsilon^{2/3}\, k^{-5/3}\, dk\,, \\ &= \frac{3}{2}\mathcal{K}\, \varepsilon^{2/3}\, k^{4/3}\,. \end{aligned} \tag{31}$$

From (31) and (30), one gets,

$$c_s = \frac{1}{\pi}\left(\frac{2}{3\mathcal{K}}\right)^{3/4}\,, \tag{32}$$

and using $\mathcal{K} = 1.5$, we arrive at

$$c_s = 0.17\,. \tag{33}$$

There are several challenges regarding the implementation of the classic Smagorinsky model:

- The first is that as put forward before, numerical models with low numerical errors are needed. In particular, the effect of the numerical dissipation error should be smaller than the Smagorinsky model, which calls for high-order models.
- The second is that the theoretical value of $c_s = 0.17$ relies on the spectrum (**??**) in homogenous turbulence at very high Re, which is usually not the case in many LES simulations. In fact, the inertial range may not appear at all in the resolved scales of motion. Subsequently, $c_s = 0.17$ is found to be too high, and typically half of this value is employed.

Dynamic estimation of the Smagorinsky constant: Problems associated with classic Smagorinsky model are usually attributed to the constant c_s. Germano et al. (1991) introduced a dynamic estimation of c_s, which works very well and considered (with variants introduced later) be to be state of the art in LES. The basic concept is that if we assume that we have the fully-resolved solution from a DNS, we should be able to estimate the appropriate value of c_s. Given that we do not have this solution, one can still devise filtering at two levels, one at the resolved LES level, and the other at a coarser level (since higher

resolution is costly), and use the information from these two filtering methods to estimate c_s as a function is time and space.

Mathematically, we know from (16) that the SGS stress that must be modeled in LES is:

$$\tau_{ij} = L_{ij} + C_{ij} + R_{ij} = \overline{u_i u_j} - \overline{u}_i \overline{u}_j \,. \tag{34}$$

A second, so-called *test filter*, denoted by operation $\widetilde{\ }$ is used, for which the SGS stresses become:

$$T_{ij} = \widetilde{\overline{u_i u_j}} - \widetilde{\overline{u}}_i \widetilde{\overline{u}}_j \,. \tag{35}$$

Note that neither τ_{ij} nor T_{ij} are known since they require knowledge of unfiltered fields.

The Leonard stress for the test filter is:

$$L_{ij} = (\widetilde{\overline{u}_i \overline{u}_j} - \widetilde{\overline{u}}_i \widetilde{\overline{u}}_j) \,. \tag{36}$$

Note that L_{ij} can be computed by filtering the LES fields. These three stresses are related by the Germano's identity:

$$L_{ij} = T_{ij} - \tau_{ij} \,. \tag{37}$$

Note that so far we have not made any assumptions on the modeling of the stresses, and in principle, the dynamic procedure can be applied to any type of model for the SGS stresses. Next, we take Smagorinsky model (28) for the unknown stress tensors τ and T

$$\tau_{ij} = -2(c_s\,\delta)^2 |\overline{S}| \overline{S}_{ij} \,, \tag{38}$$

$$T_{ij} = -2(c_s\,\widetilde{\delta})^2 |\widetilde{\overline{S}}| \widetilde{\overline{S}}_{ij} \,. \tag{39}$$

Thereby we arrive at the following relation

$$L_{ij} = -2c_s^2\,(\,\widetilde{\delta}^2\,|\widetilde{\overline{S}}|\widetilde{\overline{S}}_{ij} - \delta^2\,|\overline{S}|\overline{S}_{ij})\,, \tag{40}$$

in which everything can be computed from resolved/LES fields and the only unknown is c_s. Nevertheless, since (40) has five components, the equation is over-determined for c_s. Lilly (1992) showed that an optimal solution can be reached by using

$$c_{ds}^2 = \frac{M_{ij} L_{ij}}{M_{ij} M_{ij}} \,, \tag{41}$$

where $M_{ij} \equiv (\widetilde{\delta}^2 \, |\widetilde{\overline{S}}|\widetilde{\overline{S}}_{ij} - \delta^2 \, |\overline{S}|\overline{S}_{ij})$, and c_{ds} now denotes the dynamic coefficient, as opposed to a constant.

Nevertheless, there are problems with (41) as well. This is because turbulent flows are not at all times dissipative and the assumption of dissipative closures results in $c_{ds} < 0$, indicating backward energy cascade at certain places and times in the simulation. Most models cannot handle negative diffusivity coefficient, and this results in numerical instability. As a remedy, the following procedure is often used:

$$c_{ds}^2 = \frac{< M_{ij} L_{ij} >}{< M_{ij} M_{ij} >} \, , \quad \text{with} \quad c_{ds} = max(c_{ds}, 0) \, , \tag{42}$$

where <> indicate averaging along one of the spatial directions. Alternately, Lagrangian averaging following coherent structures could be applied (Meneveau et al., 1996). Fig. 2 shows the pdf of c_{ds} in an LES computation (Özgökmen et al., 2009a) with this dynamic estimation procedure. Note that half of the values had to be clipped since they indicated backscatter. In fact, some people think that the main improvement of the dyanmic procedure over the constant one is in its ability to set $\nu_{sgs} = 0$ in such places of the flow field. Also note that the peak of the distribution is at $c_{ds} \approx 0.08$, which is much smaller than the theoretical value of $c_s = 0.17$. Finally, values up to $c_{ds} = 0.30$ were used in this simulation at times.

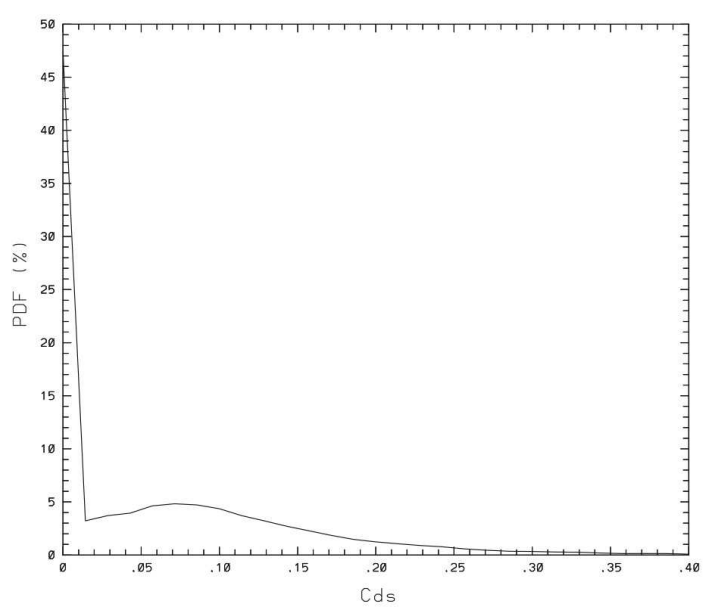

Fig. 2: Time-averaged probability distribution function of the dynamic Smagorinsky coefficient from LES of the lock-exchange problem. From p. 148 of Özgökmen et al. (2009a).

2.3 Approximate deconvolution SGS models

The *approximate deconvolution (AD)* models represent a promising alternative to the eddy-viscosity models. Instead of using physical insight to model $\tau_{ij} = \boldsymbol{\tau}(\mathbf{u}, \mathbf{u})$, the AD models are developed solely on mathematical grounds. This is highly desirable in flows where the assumptions of isotropy and homogeneity (which are essential to the assumption of energy cascade) may not hold. The main idea in approximate deconvolution is to use the available numerical approximation of $\overline{\mathbf{u}}$ to approximate $\mathbf{u}$.

2.3.1 Repeated filtering AD model:

A particular class of AD models relies on finding an approximate deconvolution of the filtered quantity by repeated filtering (Stolz and Adams, 1999), which has been shown to be an effective method for a variety of flow types, such as homogeneous transitional flows.

Let's denote by G the filter function, and by q the variables of interest. Then, $G \star q = \bar{q}$ and using $G = I - (I - G)$, the inverse of the filter can be written as the non-convergent Neumann series

$$G^{-1} \sim \sum_{i=0}^{\infty} (I - G)^i \,. \tag{43}$$

Truncating this series after N terms gives us an approximation for $G^{-1} \approx Q_N$

$$Q_N = \sum_{i=0}^{N} (I - G)^i \,, \tag{44}$$

so that the the unfiltered variable can be approximated in terms of the filtered variable using

$$q \approx q^* = Q_N \star \bar{q} \quad \textit{approximate deconvolution} \tag{45}$$

Here, as N increases, the accuracy of the inverse filter also increases:

$$\begin{aligned}
Q_1 &= I \\
Q_2 &= Q_1 + (I - G) = 2I - G \\
Q_3 &= Q_2 + (I - G)^2 = 3I - 3G + G^2 \\
Q_4 &= Q_3 + (I - G)^3 = 4I - 6G + 4G^2 - G^3 \\
Q_5 &= Q_4 + (I - G)^4 = 5I - 10G + 10G^2 - 5G^3 + G^4
\end{aligned}$$

so that

$$q \approx q^* = 5\bar{q} - 10\bar{\bar{q}} + 10\bar{\bar{\bar{q}}} - 5\bar{\bar{\bar{\bar{q}}}} + \bar{\bar{\bar{\bar{\bar{q}}}}}\,. \tag{46}$$

Since filtering can be quite expensive, it could be important that a computationally efficient filter is used for this method to be cost effective.

2.3.2 Rational AD model:

Another class of AD models are those obtained through wave-number asymptotics, such as the gradient model (Leonard, 1974). The gradient model is derived by Taylor series approximation to the Fourier transform of the Gaussian filter

$$g_\delta(\mathbf{x}) = \left(\frac{\gamma}{\pi}\right)^{\frac{3}{2}} \frac{1}{\delta^3}\, e^{-\gamma \frac{|\mathbf{x}|^2}{\delta^2}} \tag{47}$$

$$\widehat{g_\delta}(\mathbf{k}) = e^{-\frac{\delta^2|\mathbf{k}|^2}{4\gamma}} = 1 - \frac{\delta^2|\mathbf{k}|^2}{4\gamma} + \mathcal{O}(\delta^4)\,, \tag{48}$$

where $\widehat{g_\delta}(\mathbf{k})$ denotes the Fourier transform of $g_\delta(\mathbf{x})$, and its inverse is

$$\frac{1}{\widehat{g_\delta}(\mathbf{k})} = e^{\frac{\delta^2|\mathbf{k}|^2}{4\gamma}} = 1 + \frac{\delta^2|\mathbf{k}|^2}{4\gamma} + \mathcal{O}(\delta^4), \tag{49}$$

where γ is a parameter of the Gaussian filter. After a few operations (Iliescu and Fischer, 2003), it can be shown that

$$\mathbf{u} \approx \overline{\mathbf{u}} - \frac{\delta}{4\gamma}\nabla^2\overline{\mathbf{u}}\,, \tag{50}$$

and after a bit more algebra, one gets *the gradient SGS model*

$$\tau = \boldsymbol{\tau}(\mathbf{u},\mathbf{u}) = \overline{\mathbf{u}\,\mathbf{u}} - \overline{\mathbf{u}}\;\overline{\mathbf{u}} \approx \frac{\delta^2}{2\gamma}\nabla\overline{\mathbf{u}}\,\nabla\overline{\mathbf{u}}\,. \tag{51}$$

While the gradient model is shown to help preserve high wavenumber features (unlike diffusive models), it has a tendency to induce numerical instability in models. In order to address this issue, Galdi and Layton (2000) suggested so-called *rational SGS model*, denoted RLES, based on a *rational* Padé approximation, as opposed to Taylor series:

$$\widehat{g_\delta}(\mathbf{k}) = e^{-\frac{\delta^2|\mathbf{k}|^2}{4\gamma}} = \frac{1}{1 + \frac{\delta^2|\mathbf{k}|^2}{4\gamma}} + \mathcal{O}(\delta^4)\,. \tag{52}$$

The SGS stress tensor in RLES model becomes:

$$\boldsymbol{\tau}(\mathbf{u},\mathbf{u}) = \left[\left(\mathbb{I} - \frac{\delta^2}{4\gamma}\Delta\right)^{-1}\left(\frac{\delta^2}{2\gamma}\nabla\overline{\mathbf{u}}\,\nabla\overline{\mathbf{u}}\right)\right], \tag{53}$$

where $\mathbb{I}$ is the identity operator.

The RLES model (53) has been used in the numerical simulation of turbulent homogeneous flows (Iliescu and Fischer, 2003, 2004), and also for mixing in stratified flows (Özgökmen et al., 2009a,b). One of the issues in (53) is that the Helmholtz operator not only makes solution quite expensive, but also tends to over-smooth the gradient model. This problem is remedied in Özgökmen et al. (2009a) by using a reduced Helmholtz operator in which only 2 iterations are used to remove the high wavenumber features that can induce numerical instability.

2.4 Examples of LES

Next we proceed to some practical questions about testing LES, comparing different SGS models and exploring high *Re* regimes of mixing using LES.

2.4.1 What constitutes a good test problem?

Ideally, the test problem is one for which previous published literature, DNS and/or experimental results exist. If one is interested in a non-standard problem, such as mixing in stratified flows, then one may define the following criteria:

- The test problem should contain the three characteristics of stratified flows:
  - Mixing due to stably-stratified shear flows.
  - Mixing due to unstably-stratified convective motions.
  - Internal waves.

  Preferably all of them co-existing simultaneously and interacting.
- The test problem should be free from any *implicit* factors that can affect mixing, such as uncertainties in the boundary conditions, initial conditions and domain geometry.

- The test problem should be as simple as possible to set up, so that it can be used by other researchers to conduct their investigations as well.

These conditions are satisfied for the so-called- lock-exchange problem (Özgökmen et al., 2007, 2009a, 2009b).

2.4.2 Quantification of mixing:

The accuracy of the SGS models is evaluated through *a posteriori* testing. The main measure used is the background/reference potential energy (RPE), which exactly quantifies mixing in an enclosed system (Winters et al. 1995). RPE is the minimum potential energy that can be obtained through an adiabatic redistribution of the water masses. To compute RPE, we use the probability density function approach introduced by Tseng and Ferziger (2001). Specifically, we split the density perturbation field typically into 51 to 101 bins at each time step, and integrate:

$$RPE = gLW \int_0^H \rho'(z_r) z_r dz_r \,, \tag{54}$$

where $z_r(\rho')$ is the height of fluid of density ρ' in the minimum potential energy state. It is convenient to use the non-dimensional background potential energy

$$RPE^*(t^*) \equiv \frac{RPE(t^*) - RPE(0)}{RPE(0)} \,, \tag{55}$$

which shows the relative increase of the RPE with respect to the initial state by mixing.

2.4.3 What resolution constitutes an LES?

Given that LES relies on computation to capture at main eddies of a certain flows field, that change from flow to flow, depend on geometry, it is critical that the main coherent features creating turbulence are resolved. The SGS models help complete the processes of the turbulent break-down (say, in the inertial range), but they are not substitutes for all mixing, unlike RANS closures. This is depicted in Fig. 3.

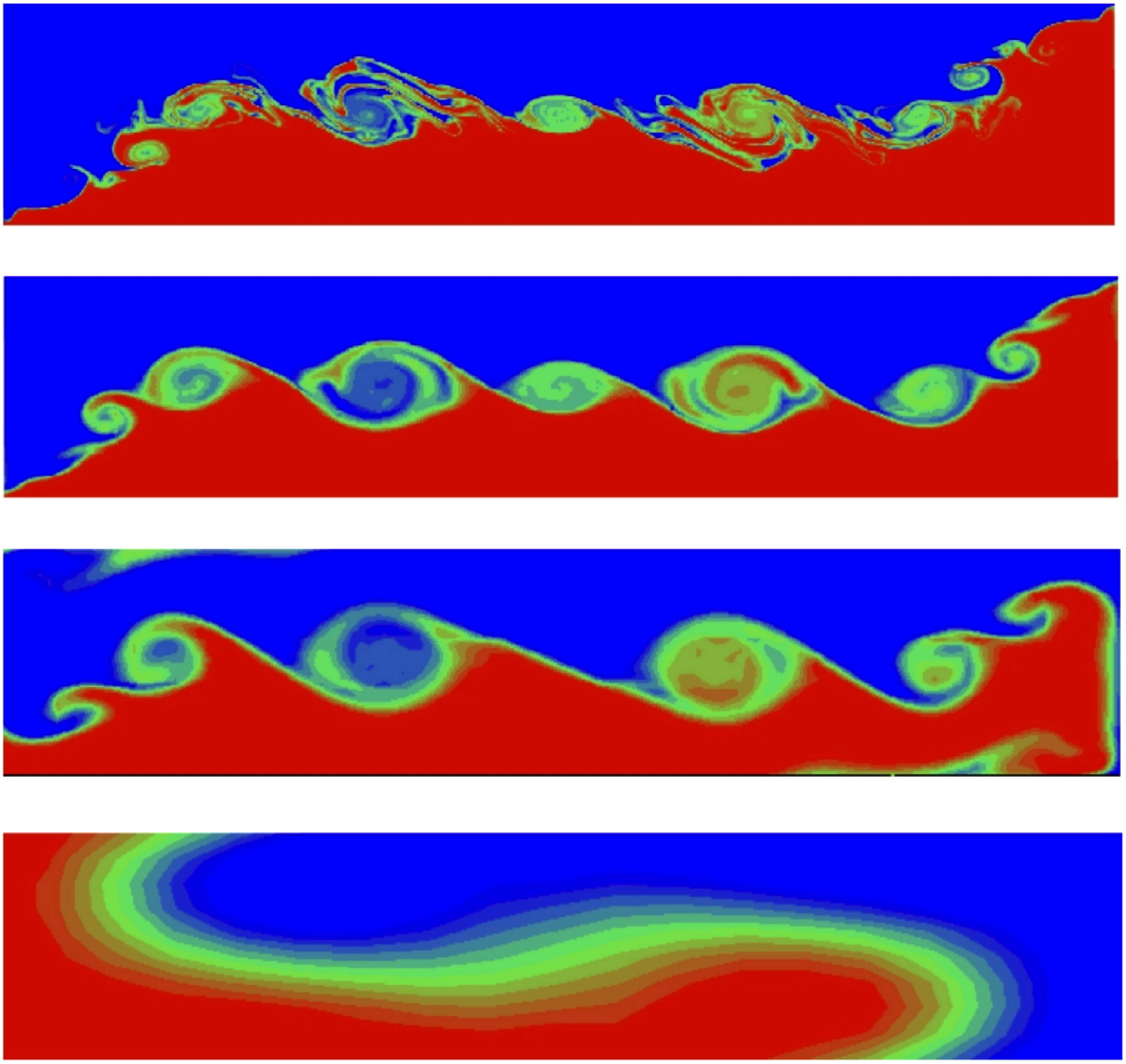

Fig. 3: Density perturbation in a 2D lock-exchange problem for different resolutions at the same time. (Top/first panel) Fully-resolved (2D DNS) simulations with 1,040,400 points; no SGS is needed. (Second panel) Simulation with 7,500 points, which captures accurately the overturning eddies, but not the smaller features imbedded in the large eddies. Simple SGS models would work fine. (Third panel) Coarser (2,700) simulation that starts to exhibit dispersion errors and misrepresents the number of large eddies. (Fourth panel) Simulations with 72 points that lacks entirely the overturning eddies and requires very comprehensive SGS models to incorporate their net effect. From Özgökmen et al. (2007).

What is the objective?

One of the objectives would be to evaluate the accuracy of different SGS models using the metric (55) and by comparing:

- DNS: fully (or highly) resolved simulations that are considered to be the gold standard for truth in computation.
- DNS*: so-called under-resolved DNS. These are coarse resolution simulations without SGS models.
- LES: coarse resolution (same resolution as DNS*) simulations with SGS models.

The main objective of LES is to attain major computation gain over DNS, typically 1000 fold in computation time, 100 fold in number of mesh points, while matching the accuracy of mixing.

Selected results at a specific Re**:** Preliminary impressions of the effect of SGS models on the solution are shown in Fig. 4. We note that classical Smagorinsky model tends to smooth the density interface, implying high diffusivity, while the rational model maintains features on the coarse mesh almost as accurately as higher resolution simulations.

Fig. 5 depicts the convergence of the mixing metric as a function of the model resolution and CPU time. Note that DNS* leads to spurious mixing which is due to the interpolation of high gradients onto a coarse resolution. The DNS* computation is about 2300 faster than DNS*, even though quite accurate solutions can be obtained with a computation that is 12 times faster than DNS.

Comparison of different SGS models is shown in Fig. 6. Perhaps the most important point is that not all SGS models improve the DNS*. Excellent agreement with DNS is obtained with an SGS model that combines the ability of dynamics Smagorinsky model to provide dissipation where and when needed with the rational model that helps preserve dispersion on coarse meshes.

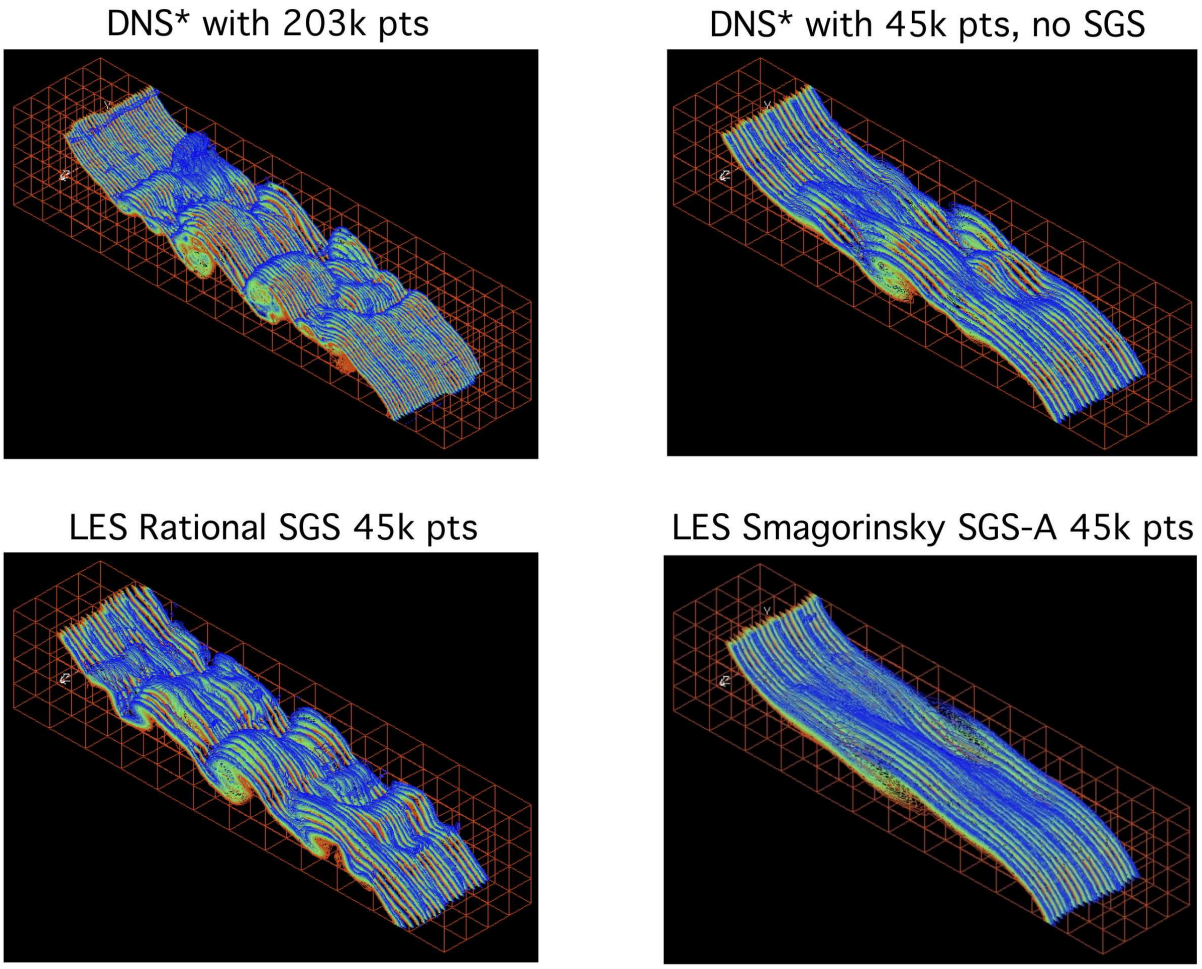

Fig. 4: Comparison of snapshots of the density perturbation field from LES with different SGS models. From Özgökmen et al. (2009a).

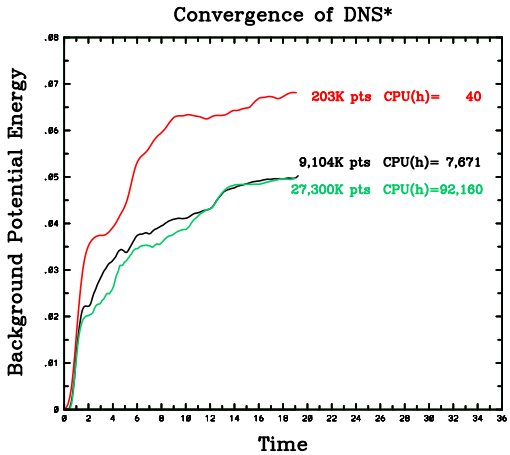

Fig. 5: Convergence of the mixing metric as a function of mesh points, and associated computation time. From Özgökmen et al. (2009a).

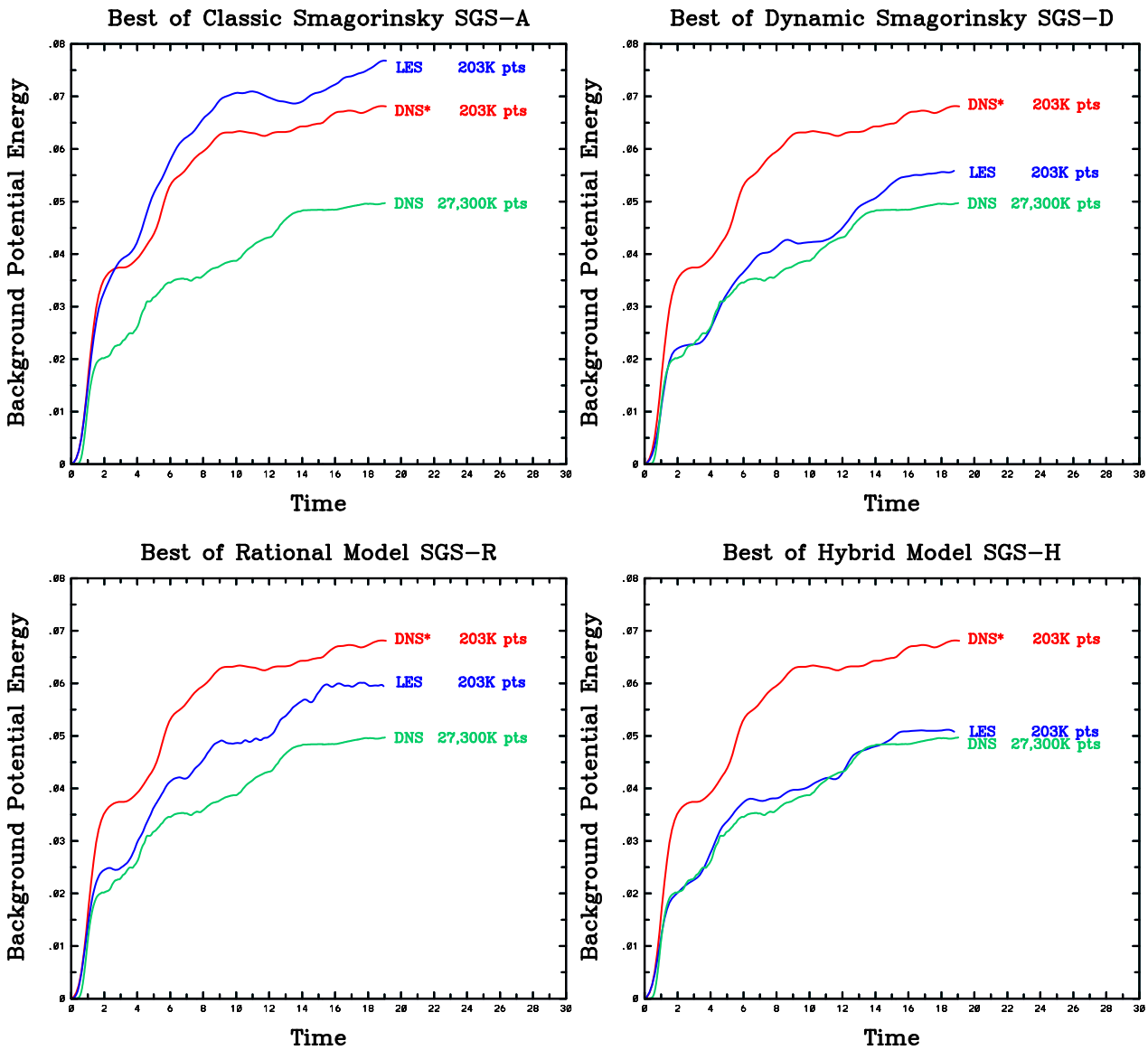

Fig. 6: Comparison of results from different SGS models in LES to those from DNS and DNS*. Note that not all SGS models lead to an improvement. The hybrid (dissipatove/dispersive) SGS model matches the mixing curve from DNS accurately while being 1200 fold cheaper computationally. From Özgökmen et al. (2009a).

Another example of repeated-filtering AD model is shown in Fig. 53.5. Here, the barotropic vorticity equation is solved for a wind-forced system, so that this case has some relevance to oceanic flows. Clearly the SGS model makes a huge difference regarding the reproduction of inertial gyres that otherwise require much higher resolution.

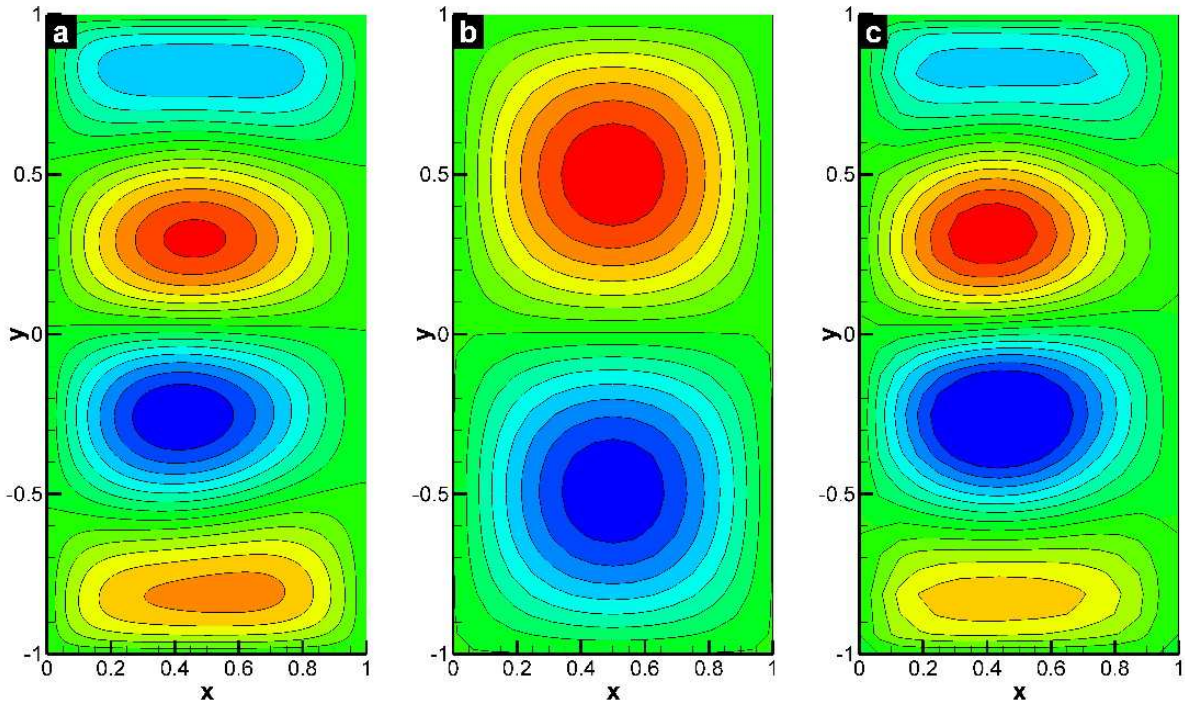

Fig. 7: Time-averaged streamfunction from a well-resolved case (left panel), under-resolved case (middle panel) and LES with repeated-filtering AD model (right panel). From San et al. (2011).

3 FTLEs from LES

A 3D FTLE code has been developed within the visualization tool visit[2] in a collaborative effort with Hank Childs, Harinarayan Krishnan (LLNL) and Christoph Garth (University of Kaiserslautern). Computations are carried out using Nek5000, a spectral element LES/DNS model developed by Paul Fischer (Argonne National Laboratory).

3.1 Application to Lock Exchange Problem

A solution to lock exchange problem (LEP) is computed using approximately 40 million mesh points. The computation was carried out over four days on 384 processors of salk, a Cray XE6m machine at CUNY high-performance computing center. An example of the FTLE field is shown in Fig. 8.

[2]visit.llnl.gov

(a) (b)

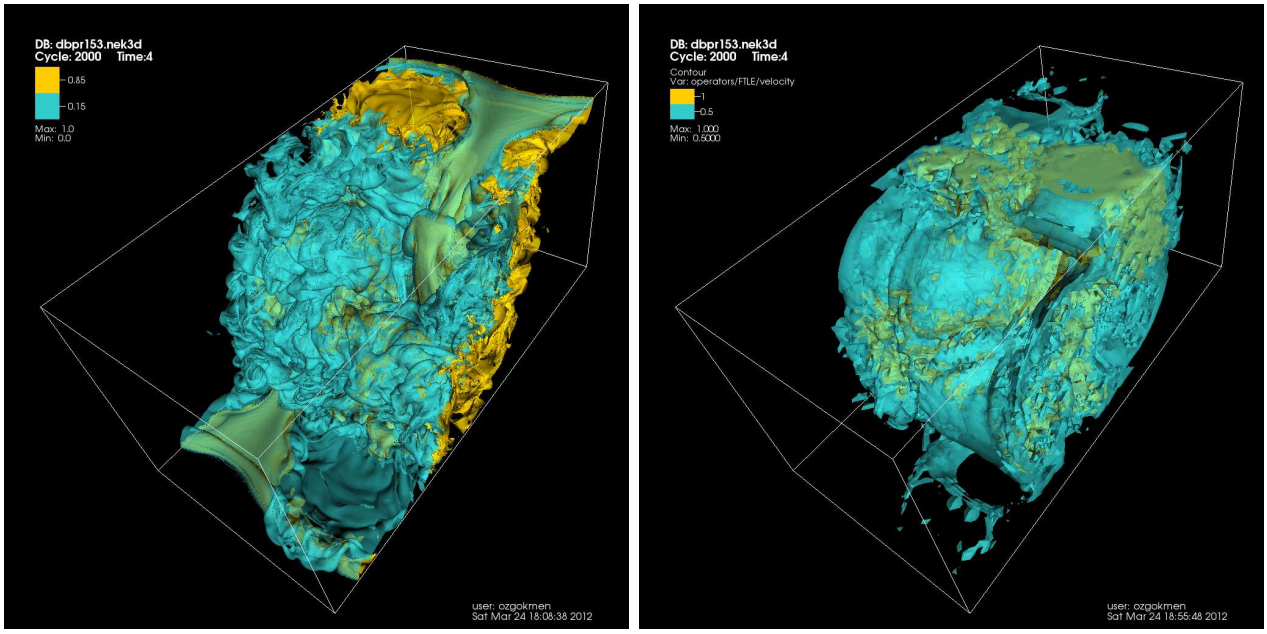

Fig. 8: The density perturbation field (left panel) and FTLE field (right panel) in LEP. The animation is available from: http://www.rsmas.miami.edu/personal/tamay/3D/dbpr153.mov

3.2 Application to Mixed Layer Instability

Mixed layer instability (MLI) is quite similar to the lock exchange problem in that the energy feeding the kinetic energy comes from the available potential energy, but there are two main differences:

- The Earth's rotation is important in MLI, leading to baroclinic instability. Subsequently, the large eddies in this problem are the coherent submesoscale eddies, as opposed to the vertical stratified overturns arising from the Kelvin-Helmholz instability in LEP.

- The main activity is constrained to a thin layer at the ocean surface, requiring computations with a very high aspect ratio, typically L/H on the O(100) to O(100). Controlling numerical diffusion through high-order numerics is important, as otherwise available potential energy can be removed by vertical diffusion, instead of the MLI.

The MLI is one of the few submesoscale motions that is relatively well understood (Mahadevan and Tandon, 2006; Boccaletti et al., 2007; Fox-Kemper et al., 2008; Thomas et al., 2008; Capet et al., 2008; Mahadevan et al., 2010; Özgökmen et al., 2011). Of particular interest is how surface submesoscale motions interact with deep mesoscale eddies. The FTLEs appear to be quite useful in gaining insight into this process (Fig. 9).

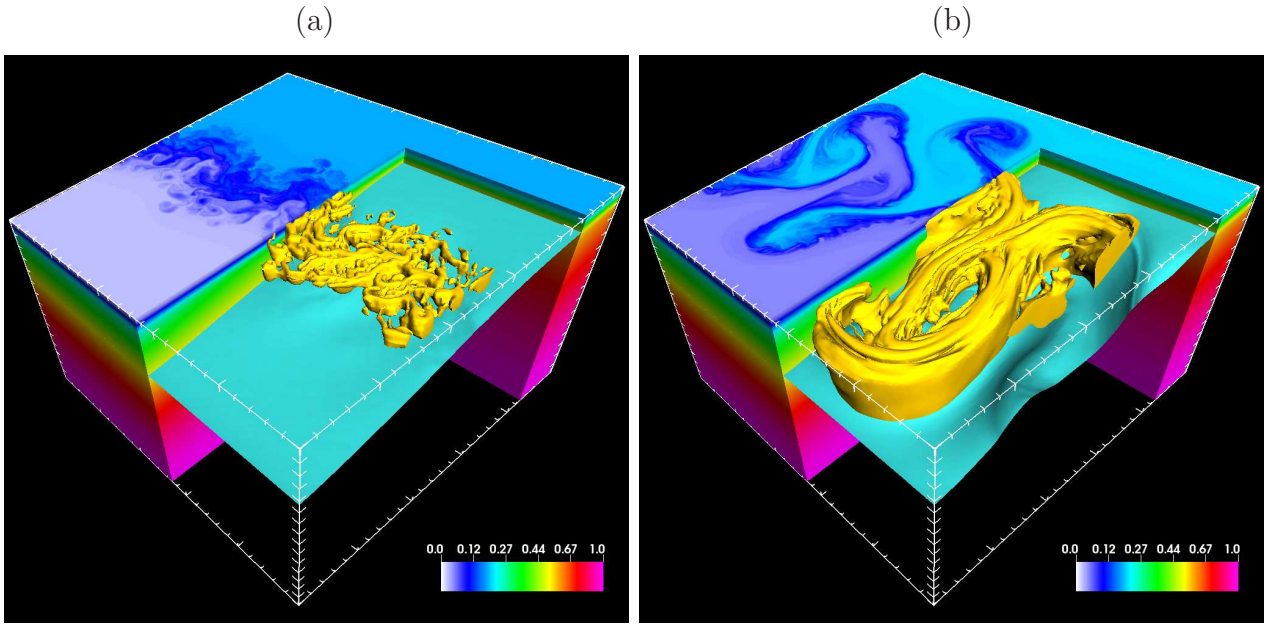

Fig. 9: The density perturbation field and FTLEs in LES during (a) the phase of MLI only, and (b) the phase when MLI and deeper baroclinic motions coexist. Surfaces corresponding to $\rho' = 0.5$ (blue) and $FTLE = 0.33$ days^{-1} (yellow) are shown. From Özgökmen et al. (2012). The animation is available from: http://www.rsmas.miami.edu/personal/tamay/3D/mlis11.mov

References

Baumert, H., Peters, H., 2004. Turbulence closure, steady state, and collapse into waves. J. Phys. Oceanogr. 34, 505–512.

Baumert, H., Simpson, J., Sündermann, J., 2005. Marine Turbulence. Cambridge University Press, Cambridge, UK.

Boccaletti, G., Ferrari, R., Fox-Kemper, B., 2007. Mixed layer instabilities and restratification. J. Phys. Oceanogr. 37, 2228–2250.

Burchard, H., Baumert, H., 1995. On the performance of a mixed-layer model based on the $k - \varepsilon$ turbulence closure. J. Geophys. Res. 100, 8523–8540.

Burchard, H., Bolding, K., 2001. Comparative analysis of four second-moment turbulence closure models for the oceanic mixed layer. J. Phys. Oceanogr. 31, 1943–1968.

Canuto, V., Cheng, Y., Howard, A., 2007. Non-local ocean mixing mode and a new plume model for deep convection. Ocean Modelling 16, 28–46.

Canuto, V. M., Howard, A., Cheng, Y., Dubovikov, M. S., 2001. Ocean turbulence. part i: One-point closure model momentum and heat vertical diffusivities. J. Phys. Oceanogr. 31, 1413–1426.

Capet, X., McWilliams, J., Molemaker, M., Shchepetkin, A., 2008. Mesoscale to submesoscale transition in the California Current System: I flow structure, eddy flux and observational tests. J. Phys. Oceanogr. 38, 29–43.

Chang, Y., Xu, X., Özgökmen, T., Chassignet, E., Peters, H., Fischer, P., 2005. Comparison of gravity current mixing parameterizations and calibration using a high-resolution 3d nonhydrostatic spectral element model. Ocean Modelling 10, 342–368.

Deville, M., Fischer, P., Mund, E., 2002. High-order methods for incompressible fluid flow. Vol. 9 of Cambridge Monographs on Applied and Computational Mathematics. Cambridge University Press, Cambridge.

Ferziger, J., 2005. Direct and large-eddy simulation of turbulence. In: Baumert, H. Z., Simpson, J. H., Sündermann, J. (Eds.), Marine Turbulence - Theories, Observations and Models. Cambridge University Press, pp. 160–181.

Fox-Kemper, B., Ferrari, R., Hallberg, R., 2008. Parameterization of mixed-layer eddies. part i: theory and diagnosis. J. Phys. Oceanogr. 38, 1145–1165.

Garrett, C., Munk, W., 1972. Space-time scales of internal waves. Geophys. Fluid Dyn. 2, 225–264.

Ilıcak, M., Özgökmen, T. M., Peters, H., Baumert, H. Z., Iskandarani, M., 2008. Performance of two-equation turbulence closures in three-dimensional simulations of the Red Sea overflow. Ocean Modelling 24, 122–139.

Kantha, L. H., Clayson, C. A., 1994. An improved mixed layer model for geophysical applications. J. Geophys. Res. 99, 252355–25266.

Kantha, L. H., Clayson, C. A., 2000. Small Scale Processes in Geophysical Flows. Academic Press, New York.

Large, W., 1998. Modeling and parameterizing the ocean planetary boundary layer. Ocean Modeling and Parameterization Chassignet, E.P and J. Verron, eds., 81–120.

Maday, Y., Patera, A. T., 1989. Spectral element methods for the Navier-Stokes equations. In: Noor, A. K. (Ed.), State of the Art Surveys in Computational Mechanics. ASME, pp. 71–143.

Mahadevan, A., Tandon, A., 2006. An analysis of mechanisms for submesoscale vertical motion at ocean fronts. Ocean Modelling 14, 241–256.

Mahadevan, A., Tandon, A., Ferrari, R., 2010. Rapid changes in the mixed layer stratification driven by submesoscale instabilities and winds. J. Geophys. Res. 115/C03017, doi:10.1029/2008JC005203.

Mellor, G. L., Yamada, T., 1982. Development of a turbulence closure model for geophysical fluid problems. Rev. Geophys. 30, 851–875.

Özgökmen, T., Poje, A., Fischer, P., Haza, A., 2011. Large eddy simulations of mixed layer instabilities and sampling strategies. Ocean Modelling 39, 311–331.

Patera, A., 1984. A spectral element method for fluid dynamics; laminar flow in a channel expansion. J. Comp. Phys. 54, 468–488.

Scotti, A., Mitran, S., 2008. An approximated method for the solution of elliptic problems in thin domains: Application to nonlinear internal waves. Ocean Modelling 25, 144–153.

Thomas, L., Tandon, A., Mahadevan, A., 2008. Submesoscale processes and dynamics. Ocean modeling in an Eddying Regime, edited by M. Hecht and H. Hasume Geophysical Monograph 177, 17–38.

Umlauf, L., Burchard, H., 2005. Second-order turbulence closure models for geophysical boundary layers. a review of recent work. Cont. Shelf Res. 25, 795–827.

Vallis, G., 2006. Atmospheric and Oceanic Fluid Dynamics. Cambridge University Press.

Warner, J. C., Sherwood, C. R., Arango, H. G., Signell, R. P., 2005. Performance of four turbulence closure methods implemented using a generic length scale method. Ocean Model. 8, 81–113.

Wilcox, D., 1998. Turbulence Modeling for CFD. DCW Industries, Inc., 2nd. edition.